NJC

PAPER

View Article Online
View Journal | View Issue

Check for updates

Cite this: New J. Chem., 2025, 49, 4801

Received 20th January 2025, Accepted 18th February 2025

DOI: 10.1039/d5nj00282f

rsc.li/njc

Unraveling boron oxidation and structure in 2D $Mo_{4/3}B_{2-x}T_z$ *via* solid-state NMR†

Yuan Zeng,[a] Hong Ma,[a] Zhongfu Tai,[a] Yan Tong,[a] Yan Wang[b] and Xiaolong Liu *[a]

Atoms from i-MAB phases are selectively etched for boridene synthesis. However, water exposure severely hinders 2D boridene formation. By using NMR techniques, we precisely uncover the oxidation mechanism of boron and gain in-depth insights into the atomic-scale properties. Our findings offer a new avenue for advancing 2D boridene research.

Since the exfoliation of graphene from graphite, two-dimensional (2D) materials have attracted extensive interest due to their inherent attributes, such as a high surface area-to-volume ratio, unique electronic structure, and diverse physicochemical properties, which make them highly suitable for applications in electronics, energy storage, and catalysis.[1] Scientists are actively growing the 2D material family to explore quantum confinement and low dimensionality.[2] Since 2011, MXenes (2D transition metal carbides, nitrides, and carbonitrides) have stood out because of their rich configurations and tunable properties.[3,4] Transition metal borides known as MBenes, formed by replacing the X element of MXenes with the neighboring B, naturally aroused increasing attention.[3,5] Because it can form multicentered bonds to overcome its electron deficiency, boron, a light element with three valence electrons, reacts strongly with metal ions.[6] Consequently, boron provides an excellent opportunity to form many intricate, multidimensional boride structures in materials. Unlike MXenes, MBenes may have notable bioactivity due to harmless boron, making them promising post-MXene materials for biotechnological applications. Although 2D MBenes are relatively new and in the early exploration stage, they are emerging as a promising class of nanomaterials.[7]

The 2D MBene family has orthorhombic and hexagonal structures, originating from MAB phases (M: transition metal, A: A-group element, and B: boron). Similar to MAX phases (layered ternary carbides and nitrides, X = C and/or N), the metallic M–A bonds in MAB phases are weaker, enabling active liquid-phase delamination.[8] The 2D material is obtained by selectively etching the A element (usually Al) out. Its one-dimensional formula is M_nB_{2n-2} (n = 2, 3, 4), with structures of alternating transition metal and B layers. Besides these typical MBenes, there are also fourteen predicted $(M'_{2/3}M''_{1/3})_2B_2$ MBenes, where M′ includes Ti, Cr, Mn, Fe, Mo, and W and M″ includes Sc, Y, Zr, Nb, and Hf,[9] along with high-entropy MAB/MAX phases[10] and M_2AlB_2 structures.[11,12]

Finding a suitable precursor susceptible to deintercalation has proven difficult in the search for 2D MBenes. Recently, quaternary 3D i-MAB (in-plane chemical ordering) phases like $Mo_{4/3}Y_{2/3}AlB_2$ and $Mo_{4/3}Sc_{2/3}AlB_2$ were synthesized.[13] Binary MBenes with ordered vacancies can be fabricated by etching light transition metals and Al from i-MAB phases. In the resultant molybdenum boride, vacancies emerge at the Y or Sc atom sites of the parent structure. These vacancies alter the electronic band and optical properties, impacting conductivity, bandgap, and absorption.[14] Ordered vacancies can influence the diffusion and transport of ions within molybdenum borides, making them promising candidates for applications in energy storage devices, such as batteries and supercapacitors.[15] 2D MBenes are 2D honeycomb boron layers doped with transition metals. Electron localization functions (ELFs) clearly show electron localization between neighboring B–B atomic pairs, suggesting covalent bonding interactions among boron atoms in the planar layer of molybdenum boride.[16] 2D boridene in molybdenum boride resembles graphene to an extent. As a single-layer boron material, it's less stable than graphene and other 2D counterparts, hampering its development. Boridene oxidizes rapidly in air due to high oxygen reactivity, degrading its properties. It also reacts with water, yielding boron oxides. To obtain boridene, selective etching extracts specific atoms from i-MAB phases. Water exposure during etching is almost inevitable, especially with aqueous solutions. The reactive 2D boron atoms readily react with water, changing the

[a] School of Materials, Sun Yat-sen University, Shenzhen, Guangdong 518107, China. E-mail: liuxlong9@mail.sysu.edu.cn
[b] Instrumental Analysis and Research Center, Sun Yat-sen University, Guangzhou, Guangdong 510275, China

† Electronic supplementary information (ESI) available: Experimental procedures and other data. See DOI: https://doi.org/10.1039/d5nj00282f

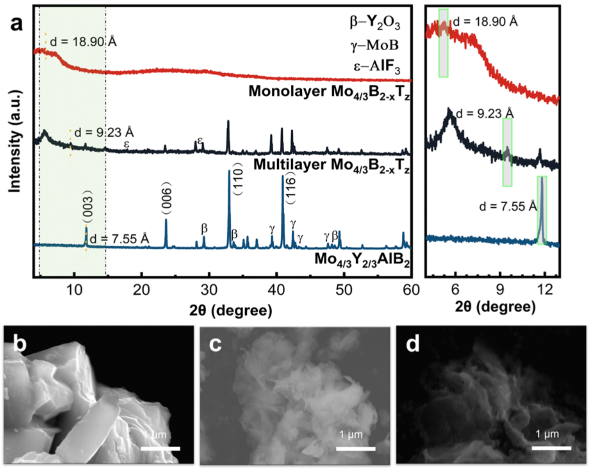

Fig. 1 (a) XRD patterns of 3D $(Mo_{2/3}Y_{1/3})_2AlB_2$ and its 2D derivative $Mo_{4/3}B_{2-x}T_z$ (monolayer and multilayer boridene); (b) SEM picture of 3D $(Mo_{2/3}Y_{1/3})_2AlB_2$; (c) SEM picture of multilayer $Mo_{4/3}B_{2-x}T_z$ boridene; and (d) SEM picture of monolayer $Mo_{4/3}B_{2-x}T_z$ boridene.

boridene structure. Since 2D molybdenum boride is in the early development phase, its properties demand further study. Thus, this work utilized SSNMR, XPS, and IR for a comprehensive composition analysis.

$(Mo_{2/3}Y_{1/3})_2AlB_2$ compounds were prepared according to ref. 14 by a solid-state reaction of elemental powders. Through HF-etching, 2D $Mo_{4/3}B_{2-x}T_z$, where T_z is fluorine, oxygen, or hydroxide surface terminations, was obtained by removing the Al and Y/Sc atoms and a small amount of B atoms.[14] Generally, the relative intensity of the newly formed lower angle (00l) peak increased with the increasing HF concentration and etching time. Because 2D $Mo_{4/3}B_{2-x}T_z$ materials are sensitive to the environment, especially in concentrated HF solutions, shorter etching times and lower HF concentrations are preferred to obtain 2D ribbons with higher quality and stability. The corresponding XRD results of the etched powders are shown in Fig. 1a. After the HF treatment, there has been a significant decrease in the peak intensities originating from the $(Mo_{2/3}Y_{1/3})_2AlB_2$ precursor. The (001) peak downshifts to a lower angle of $2\theta = 9.35°$, corresponding to an enlarged *d*-spacing value (*d*) of 9.23 Å, from the original 7.55 Å for $(Mo_{2/3}Y_{1/3})_2AlB_2$. This additional low-angle (001) peak is frequently seen for MXenes that are made by selectively etching a MAX phase in HF.[3,5] To investigate the morphology of the synthesized samples, the microstructure of 2D $Mo_{4/3}B_{2-x}T_z$ was observed by SEM and is shown in Fig. 1c and d. The morphology of monolayer $Mo_{4/3}B_{2-x}T_z$ films appears to be ribbon-like. The transition from a bulk phase to a layered material shows notable crystal structure and morphology changes due to selective etching.

A microscopic investigation (Fig. S1, ESI†) has been performed to study the topochemical deintercalation of Al and Y from $(Mo_{2/3}Y_{1/3})_2AlB_2$ crystals by using transmission electron microscopy (TEM). An isolated 2D $Mo_{4/3}B_{2-x}T_z$ monolayer was observed in Fig. S1c (ESI†), suggesting that the synthesis and exfoliation of MBenes are feasible. The pristine 2D molybdenum boride should be $Mo_{4/3}B_2$ without surface termination. TEM images of $Mo_{4/3}Y_{2/3}AlB_2$ demonstrate that each 2D $Mo_{4/3}B_2$ monolayer consists of boron layers sandwiched with molybdenum layers, *i.e.*, three atomic layers stacked as Mo–B–Mo.[17] Scheme S1 (ESI†) demonstrates the sandwich structure of 2D $Mo_{4/3}B_2$. Raman spectroscopy is recognized as a robust, non-destructive technique for characterizing low-dimensional materials. Raman spectroscopy is employed to reveal the remarkable structure of monolayer $Mo_{4/3}B_{2-x}T_z$. Raman spectral measurements of 2D $Mo_{4/3}B_{2-x}T_z$ are shown in Fig. S2 (ESI†). Multiple Raman peaks are found at around 188, 337, 808, and 967 cm^{-1} for monolayer $Mo_{4/3}B_{2-x}T_z$. The two intense peaks at 808 and 967 cm^{-1} could be assigned to the covalent B–B vibration of the boridene sheet in monolayer $Mo_{4/3}B_{2-x}T_z$.[18] Meanwhile, these peaks might be related to other types of vibrational modes in the material. The intense peaks at 188 cm^{-1} and 337 cm^{-1} could be attributed to B–O and Mo–B vibrations, respectively.[19] Due to the electron deficiency, the boron-based graphene-like honeycomb materials cannot exist stably. The above observations indicate that covalent bonds between B atoms create a particular 2D borophene-like B layer that is bonded to MoB_2 frameworks and does not exist in isolated forms.

The experimentally determined chemical formula of molybdenum boride, $Mo_{4/3}B_{2-x}T_z$, indicates the possible existence of boron vacancies, and the concentration of the unknown surface termination group (T) remains undetermined. As our experimental investigations have shown, these surface groups play a crucial role in the stability and significantly influence many other materials applications. The XPS measurements have been employed to identify the chemical states (binding energies (BEs)) of those constituting elements in the $(Mo_{2/3}Y_{1/3})_2AlB_2$ precursor and the filtered $Mo_{4/3}B_{2-x}T_z$ film.[14] The XPS spectrum of monolayer $Mo_{4/3}B_{2-x}T_z$ is shown in Fig. 2. In Fig. 2a, four peaks fit the Mo 3d region for the $Mo_{4/3}B_{2-x}T_z$ film, and the peaks correspond to Mo species belonging to the $Mo_{4/3}B_{2-x}T_z$ sheets with oxidized states of Mo^{4+}, Mo^{5+}, and Mo^{6+}. Fig. 2b presents the XPS spectrum of the B 1s region for the film, where the spectrum is fitted by two species: one belonging to $Mo_{4/3}B_{2-x}T_z$ sheets and the other one corresponding to B_2O_3 surface oxide. Based on the XPS measurements and analysis, it can be found that almost all of the Y atoms are removed, in addition to the complete removal of Al atoms during etching. Furthermore, in Fig. S3 (ESI†), surface terminations T_z were a mixture of –O, –OH, and –F based on the XPS spectra of O 1s and F 1s of the $Mo_{4/3}B_{2-x}T_z$ sheets. A previous XPS analysis of a freestanding film also suggests that

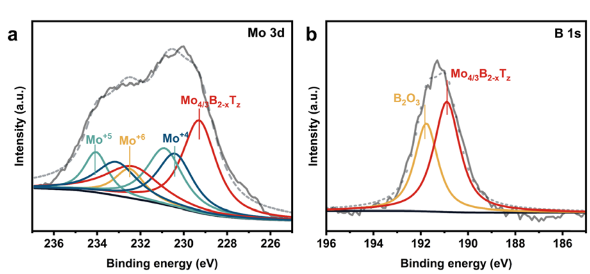

Fig. 2 High-resolution XPS spectra of monolayer $Mo_{4/3}B_{2-x}T_z$: (a) the Mo 3d region and (b) the B 1s region, and their fittings representing various species.

the three termination types O, F, and OH are present.[14,20] Due to the synthesis of MBenes through wet etching approaches, the existence of surface terminations on the outer MBenes' surface and between the layers is inevitable, and the surface terminations including –O, –OH, and –F groups will be present for MBenes.[20] Although the surface chemistry's effect is considered minor for most macroscopic materials, it is crucial for 2D nanomaterials due to their massive lateral diameters and unusual surface areas.[6]

Our XRD and XPS observations are consistent with the findings reported in Science.[10] In that paper, XPS offered valuable surface chemistry and bonding data, especially for boron and molybdenum. As a surface analysis technique, XPS details the chemical composition, oxidation states, and electronic states of surface elements, probing only the top 1–10 nm. XPS spectra show elemental composition and chemical states at specific surface points or regions. Solid-state NMR, in contrast, is a bulk characterization method. It covers the whole sample, both surface and interior, and is great for studying atomic-scale nucleus structure, dynamics, and chemical environments. Thus, it gives comprehensive bulk details about a material's atomic-scale structural and dynamic properties.

Indeed, these oxides may localize on the surface. Such surface localization can cause high intensity in the XPS spectrum, perhaps masking the underlying boride material. So, though boron oxide seems to dominate the surface chemistry seen in XPS, the underlying monolayer hydrogenated boride may still exist beneath the oxide layer. Solid-state NMR is valuable for studying bulk information, especially useful for crystalline, amorphous materials, surfaces, interfaces, and heterogeneous systems. It can also offer details about local environments, chemical bonding, and atomic-scale structure. Since the bond nature of MAB phases is crucial for MBene synthesis, thorough experimental research on it is urgently needed.

Due to the ability of ^{11}B and ^{27}Al solid-state NMR spectroscopy to provide diverse chemical information, ^{11}B and ^{27}Al NMR spectroscopies are indispensable tools for characterizing MAB phases. Since ^{11}B and ^{27}Al are quadrupolar nuclei with half-integral spin (3/2 and 5/2), operation at high magnetic field strength causes only the central (1/2, −1/2) transition to be observed. Fig. 3(a) and Fig. S4 (ESI†) show the ^{11}B and ^{27}Al MAS NMR spectra of $Mo_{4/3}Y_{2/3}AlB_2$, multilayer $Mo_{4/3}B_{2-x}T_z$ and monolayer $Mo_{4/3}B_{2-x}T_z$. To eliminate interference from the probe components (rotors), the ^{11}B MAS NMR spectra of the boride materials comprise different spectra of them and the spectrum of an empty rotor, all obtained using the same experimental conditions. The ^{27}Al chemical shift of $Mo_{4/3}Y_{2/3}AlB_2$ is around 184 ppm, which indicates that aluminum atoms form metallic bonds within the layered structure. Only a few aluminum oxides with −5.0 ppm were observed after the deintercalation process of Al from $Mo_{4/3}Y_{2/3}AlB_2$ crystals.

According to the reference, the 15 ppm and 1.5 ppm signals in ^{11}B MAS NMR spectra correspond to BO_3 and BO_4 units in boron-containing materials, respectively.[21] Relying solely on chemical shifts often doesn't provide convincible assignments, especially in complex materials. To overcome the limitations of

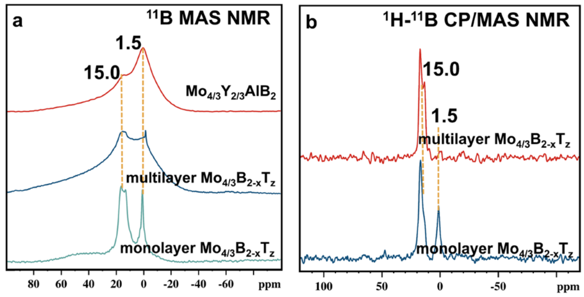

Fig. 3 (a) ^{11}B MAS NMR spectra of $Mo_{4/3}Y_{2/3}AlB_2$, multilayer $Mo_{4/3}B_{2-x}T_z$, and monolayer $Mo_{4/3}B_{2-x}T_z$. (b) ^{1}H−^{11}B CP/MAS NMR spectra of multilayer $Mo_{4/3}B_{2-x}T_z$ and monolayer $Mo_{4/3}B_{2-x}T_z$.

^{11}B MAS for signal assignment, ^{1}H–^{11}B CP/MAS, ^{1}H–^{11}B (HETeronuclear CORrelation) HETCOR, and ^{11}B–^{11}B proton-driven spin diffusion (PDSD) techniques have been employed to study structural correlations between boron and hydrogen, as well as between different boron species. HETCOR often gives a more detailed picture of heteronuclear proximities (*e.g.*, boron and protons), whereas PDSD excels in exploring homonuclear couplings (*e.g.*, ^{11}B–^{11}B). HETCOR reveals heteronuclear interactions (*e.g.*, ^{1}H–^{11}B), which provides more detailed insights into the local bonding environment, particularly the relationship between boron centers and surrounding protons. PDSD reveals spatial proximities and connects nearby atoms within the same spin system, making it valuable for understanding short- and medium-range structures. In this case, PDSD can be a valuable technique to explore the spatial proximity between boron atoms, especially B–B interactions.

The ^{1}H–^{11}B CP/MAS and ^{1}H–^{11}B HETCOR NMR techniques have been used to characterize the hydrogen–boron interactions, providing valuable insights into the chemical environment of boron atoms in hydroxylated terminations. The ^{11}B resonance peak in Fig. 3b and the correlated signals in Fig. S5 (ESI†) provide valuable information about a sample's spatial proximity and interactions between hydrogen and boron atoms in multilayer $Mo_{4/3}B_{2-x}T_z$ and monolayer $Mo_{4/3}B_{2-x}T_z$. The correlated contour in Fig. 3b demonstrates the spatial correlation between a proton with a chemical shift around +9 ppm and B with a chemical shift around +15 ppm. The correlated signal indicates that B–OH···OB hydrogen bonds spatially connect BO_3 units. The correlated signals in Fig. 4a indicate that the protons in both B–OH···OB hydrogen bonds and B–OH groups are spatially close to the BO_3 and BO_4 units in monolayer $Mo_{4/3}B_{2-x}T_z$, respectively. The protons in monolayer $Mo_{4/3}B_{2-x}T_z$ created an H-bonded network, which chemically bonded or structurally integrated the oxidized boron species into the primary 2D $Mo_{4/3}B_{2-x}T_z$ structure. The first-principles calculations showed that surface functionalization improves the dynamical stability of the boridene sheets.[16] Oxidized boron stabilized the 2D $Mo_{4/3}B_{2-x}T_z$ material under ambient conditions, preventing further degradation or oxidation of the Mo or B atoms.

Besides HETCOR, proton-driven spin diffusion (PDSD) is highly effective for probing spatial proximity, especially in B–B interactions in boridene. However, no B–B correlated peaks

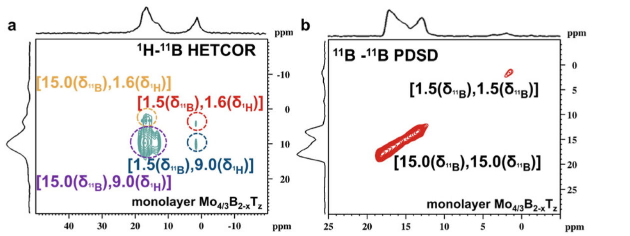

Fig. 4 (a) ^{1}H–^{11}B HETCOR NMR and (b) ^{11}B–^{11}B PDSD NMR spectra of monolayer $Mo_{4/3}B_{2-x}T_z$.

have been observed in Fig. 4b. The self-correlated signals in Fig. 4b between the same type of boron nuclei (*e.g.*, BO_3 or BO_4 groups) suggest that these boron atoms are in close spatial proximity within the same phase or structural environment. The boron atoms in boridene are in close spatial proximity within the same structural environment. However, the absence of correlated peaks other than BO_3 or BO_4 groups in Fig. 4b suggests that there are no B–B interactions within the detectable range of the experiment. The lack of inter-site interactions between different boron environments, *i.e.*, BO_3 *vs.* BO_4, implies that little spatial interaction exists between these distinct boron environments in the material. NMR spectra show that borate-like or borax-like species were formed when boron sources partially oxidized and created discrete layers or clusters during synthesis or post-processing. Then, multiple ^{11}B NMR techniques have been performed on boric acid (H_3BO_3) in Fig. S6 (ESI†) and borax (sodium borate, $Na_2B_4O_7{\cdot}10H_2O$) in Fig. S7 (ESI†) further to clarify the oxidation species in 2D $Mo_{4/3}B_{2-x}T_z$. Fig. S6 (ESI†) demonstrates that boric acid primarily consists of boron in a trigonal BO_3 configuration. The three-coordinate trigonal planar structure of boron (BO_3) has a broadened line shape due to quadrupolar coupling for environments with lower symmetry. Fig. S7 (ESI†) exhibits similarities to the NMR spectra of monolayer $Mo_{4/3}B_{2-x}T_z$. The ^{11}B chemical shifts around 15.0 ppm correspond to BO_3 units, and the ^{11}B resonance peak at 1.5 ppm could be attributed to BO_4 units. Based on the NMR spectra of H_3BO_3 and borax, it is observed that during the etching process of light transition metal atoms and Al from the i-MAB phases, boron–oxygen bonds (such as BO_3 or BO_4 units) are formed. The formation mechanism proceeds from $Mo_{4/3}Y_{2/3}AlB_2$ and $Mo_{4/3}Sc_{2/3}AlB_2$ to the formation of $Mo_{4/3}B_{2-x}(OH)_z$, alongside the generation of $AlF_3{\cdot}xH_2O$ and $YF_3{\cdot}xH_2O$. This process demonstrates the role of boron–oxygen bond formation in stabilizing the structure during oxidation, preventing further degradation of the Mo or B atoms in the 2D material. The similarity between the ^{11}B NMR spectra of borax and monolayer $Mo_{4/3}B_{2-x}T_z$ is that they both have boron in trigonal (BO_3) and tetrahedral (BO_4) habitats. Multiple ^{11}B NMR spectra suggest that most boron atoms in $Mo_{4/3}B_{2-x}T_z$ could be oxidized into BO_3 and BO_4 units. Boridene is inherently sensitive to oxidation, thermal conditions, and environmental factors, which can lead to degradation over time. Advances in controlled etching environments, protective strategies, and alternative techniques are essential to overcome these challenges and achieve stable boride with desirable properties. The observed ^{11}B MAS NMR signals mainly come from borate-like species, helping to clarify the actual structure of the 2D $Mo_{4/3}B_{2-x}T_z$ materials.

Bulk boron does not have a simple layered structure like graphite (the precursor to graphene). Instead, boron forms complex, three-dimensional structures with strong covalent bonds between atoms, making it different from materials like graphite or molybdenum disulfide (MoS_2), where layers can be easily separated into 2D sheets.[22] Boridene's metastability arises from the nonlayered structure of bulk boron, making it inherently less stable than materials like graphene. This metastability requires careful synthesis and handling to maintain boridene in its 2D form. Boridene's synthesis often requires careful control of experimental conditions, such as temperature and the choice of substrate, to stabilize the 2D form.[23,24] Typically, 2D materials are synthesized by exfoliating van der Waals solids, but boridene is an exception, produced through the selective etching of aluminum and yttrium (or scandium) from chemically ordered 3D compounds like $(Mo_{2/3}Y_{1/3})_2AlB_2$ and $(Mo_{2/3}Sc_{1/3})_2AlB_2$. The etching process in aqueous hydrofluoric acid selectively removes Al and Y/Sc, leaving $Mo_{4/3}B_{2-x}$ sheets terminated with fluorine, oxygen, or hydroxide (T_z). The possibility of synthesizing a wide variety of 2D transition metal borides through chemical exfoliation of laminated materials may expand the toolkit of 2D materials beyond conventional van der Waals solids or MXenes. However, NMR results confirm the formation of boron–oxygen bonds (*e.g.*, BO_3 or BO_4 units), which prevents further oxidation or degradation of the underlying Mo or B atoms in the 2D material. By preventing deep oxidation or corrosion of the Mo and B atoms, the oxidized boron species help maintain the overall structural integrity of the 2D material. The etching process to produce "boridene" from i-MAB phases is delicate and dramatically influences the resulting material's stability.

In summary, 2D $Mo_{4/3}B_{2-x}$ MBenes with ordered vacancies were made by etching light transition metals and Al from i-MAB phases. Combining solid-state NMR and other methods, we probed the structural and chemical properties of MAB phases and their exfoliated products. Results show that materials change greatly during wet-chemical etching and delamination. Most B atoms in multilayer and monolayer $Mo_{4/3}B_{2-x}$ oxidize. Grasping boridene-environment interactions is key for applications. These findings expand our understanding of synthesis and lay a foundation for exploring atomically thin materials.

Author contributions

Yuan Zeng: writing – original draft, investigation; Hong Ma: data curation and analysis; Zhongfu Tai and Yan Tong: reviewing and editing; Yan Wang: visualization; and Xiaolong Liu: writing – reviewing and editing, methodology, funding acquisition.

Data availability

Data are available on reasonable request.

Conflicts of interest

There are no conflicts to declare.

Acknowledgements

This research was financially supported by the National Natural Science Foundation of China (NSFC) (22075322).

Notes and references

1 K. S. Novoselov, A. K. Geim, S. V. Morozov, D. Jiang, Y. Zhang, S. V. Dubonos, I. V. Grigorieva and A. A. Firsov, *Science*, 2004, **306**, 666–669.
2 S. Z. Butler, S. M. Hollen, L. Cao, Y. Cui, J. A. Gupta, H. R. Gutiérrez, T. F. Heinz, S. S. Hong, J. Huang, A. F. Ismach, E. Johnston-Halperin, M. Kuno, V. V. Plashnitsa, R. D. Robinson, R. S. Ruoff, S. Salahuddin, J. Shan, L. Shi, M. G. Spencer, M. Terrones, W. Windl and J. E. Goldberger, *ACS Nano*, 2013, **7**, 2898–2926.
3 M. Naguib, M. Kurtoglu, V. Presser, J. Lu, J. Niu, M. Heon, L. Hultman, Y. Gogotsi and M. W. Barsoum, *Adv. Mater.*, 2011, **23**, 4248–4253.
4 B. Anasori, M. R. Lukatskaya and Y. Gogotsi, *Nat. Rev. Mater.*, 2017, **2**, 16098.
5 M. Naguib, O. Mashtalir, J. Carle, V. Presser, J. Lu, L. Hultman, Y. Gogotsi and M. W. Barsoum, *ACS Nano*, 2012, **6**, 1322–1331.
6 H. Braunschweig and M. Colling, *Coord. Chem. Rev.*, 2001, **223**, 1–51.
7 M. Jakubczak, A. Szuplewska, A. Rozmysłowska-Wojciechowska, A. Rosenkranz and A. M. Jastrzębska, *Adv. Funct. Mater.*, 2021, **31**, 2103048.
8 X. Liu, X. Ge, Y. Dong, K. Fu, F. Meng, R. Si, M. Zhang and X. Xu, *Mater. Chem. Phys.*, 2020, **253**, 123334.
9 Y. Yao, N. Miao, Y. Gong and J. Wang, *Nanoscale*, 2021, **13**, 13208–13214.
10 Z. Du, C. Wu, Y. Chen, Q. Zhu, Y. Cui, H. Wang, Y. Zhang, X. Chen, J. Shang, B. Li, W. Chen, C. Liu and S. Yang, *Adv. Energy Mater.*, 2022, **12**, 2103228.
11 L. T. Alameda, R. W. Lord, J. A. Barr, P. Moradifar, Z. P. Metzger, B. C. Steimle, C. F. Holder, N. Alem, S. B. Sinnott and R. E. Schaak, *J. Am. Chem. Soc.*, 2019, **141**, 10852–10861.
12 T. Yilmaz, O. G. Yildiz, N. S. Peighambardoust, M. Baitinger and U. Aydemir, *Inorg. Chem.*, 2025, **64**, 1139–1145.
13 J. Zhou, J. Palisaitis, J. Halim, M. Dahlqvist, Q. Tao, I. Persson, L. Hultman, P. O. Å. Persson and J. Rosen, *Science*, 2021, **373**, 801–805.
14 K. Kim, C. Chen, D. Nishio-Hamane, M. Okubo and A. Yamada, *Chem. Commun.*, 2019, **55**, 9295–9298.
15 B. Chen, H. Liu, T. Bai, Z. Song, J. Xie, K. Wu, Y. Cheng and B. Xiao, *Nanoscale*, 2022, **14**, 17955–17975.
16 H. Wu, Z. Gao, F. Ma, Z. Tian, Y. Liu, Y. Jiao and A. Du, *Appl. Surf. Sci.*, 2022, **602**, 154374.
17 M. Dahlqvist, Q. Tao, J. Zhou, J. Palisaitis, P. O. Å. Persson and J. Rosen, *J. Am. Chem. Soc.*, 2020, **142**, 18583–18591.
18 A. Sarycheva and Y. Gogotsi, *Chem. Mater.*, 2020, **32**, 3480–3488.
19 S. Sahoo and S. K. Singh, *Ceram. Int.*, 2017, **43**, 15561–15566.
20 M. Khazaei, J. Wang, M. Estili, A. Ranjbar, S. Suehara, M. Arai, K. Esfarjani and S. Yunoki, *Nanoscale*, 2019, **11**, 11305–11314.
21 S. Geng, F. U. Shah, P. Liu, O. N. Antzutkin and K. Oksman, *RSC Adv.*, 2017, **7**, 7483–7491.
22 X. Sun, X. Liu, J. Yin, J. Yu, Y. Li, Y. Hang, X. Zhou, M. Yu, J. Li, G. Tai and W. Guo, *Adv. Funct. Mater.*, 2017, **27**, 1603300.
23 B. Feng, J. Zhang, Q. Zhong, W. Li, S. Li, H. Li, P. Cheng, S. Meng, L. Chen and K. Wu, *Nat. Chem.*, 2016, **8**, 563–568.
24 B. Kiraly, X. Liu, L. Wang, Z. Zhang, A. J. Mannix, B. L. Fisher, B. I. Yakobson, M. C. Hersam and N. P. Guisinger, *ACS Nano*, 2019, **13**, 3816–3822.